

Self-guiding electromagnetic beams in relativistic electron–positron plasmas

T. Tatsuno^{a,b}, M. Ohhashi^a, V.I. Berezhiani^{a,c,*}, S.V. Mikeladze^c

^a Graduate School of Frontier Sciences, The University of Tokyo, Kashiwa, Chiba 277-8561, Japan

^b Center for Scientific Computation and Mathematical Modeling, The University of Maryland, College Park, MD 20742-3289, USA

^c Institute of Physics, 6 Tamarashvili, Tbilisi 0177, Georgia

Received 15 September 2006; received in revised form 27 October 2006; accepted 30 October 2006

Available online 7 November 2006

Communicated by V.M. Agranovich

Abstract

Nonlinear interaction of an intense electromagnetic (EM) beam with relativistically hot electron–positron plasma is investigated by invoking the variational principle and numerical simulation, resting on the model of generalized nonlinear Schrödinger equation with saturating nonlinearity. The present analysis shows the dynamical properties including the possibilities of trapping and wave-breaking of EM beams. These properties of EM beams may give a significant clue for the gamma-ray burst.

© 2006 Elsevier B.V. All rights reserved.

PACS: 52.27.Ep; 52.27.Ny; 52.35.Mw; 98.70.Rz

Keywords: Electron–positron plasma; Special relativity; Gamma-ray burst; Nonlinear Schrödinger equation; Saturating nonlinearity; Variational principle

1. Introduction

The problem of electromagnetic (EM) wave propagation and related phenomena in relativistic plasma have attracted considerable attention in the recent past. Relativistic electron–positron (e–p) dominated plasmas are created in a variety of astrophysical situations. Electron–positron pair production cascades are believed to occur in pulsar magnetospheres [1]. The e–p plasmas are also likely to be found in the bipolar outflows (Jets) in active galactic nuclei (AGN) [2], and at the center of our own Galaxy [3]. In AGNs, the observations of superluminal motions are commonly attributed to the expansion of relativistic e–p beams in a pervading subrelativistic medium. This model implies copious pair production via γ – γ interactions creating an e–p atmosphere around the source. The actual production of e–p pairs due to photon–photon interactions occurs in the coronas of AGN accretion disks, which upscatter the soft photons emitted by the accretion disks by inverse Compton scattering.

The presence of e–p plasma is also argued in the MeV epoch of the early Universe [4]. On the other hand the contemporary progress in the development of super-strong laser sources with intensities $I = 10^{21-23}$ W/cm² has also made it possible to create relativistic e–p plasmas in the laboratory by a variety of experimental techniques [5]. Elucidation of the electromagnetic wave dynamics in a relativistic e–p plasmas will, perhaps, be an essential determinant of the radiation properties of astrophysical objects as well as of the medium exposed to the field of super-strong laser radiation.

Wave self-modulation and soliton-formation is, perhaps, one of the most interesting and significant features of the overall plasma dynamics. The existence of stable localized envelope solitons of EM radiation has been suggested as a potential mechanism for the production of micro-pulses in AGN and pulsars [6–8]. In the early Universe localized solitons are strong candidates to explain the observed inhomogeneities of the visible Universe [9,10], and vortex soliton can be considered to play a significant role for the formation of the observed structure of the Universe [11]. The gamma-ray bursts (GRBs) and their afterglows are likely to be the result of energy dissipation from a relativistically expanding outflow [12]. A pointing-

* Corresponding author.

E-mail address: vazhab@yahoo.com (V.I. Berezhiani).

flux driven outflow from a magnetized rotator is a promising paradigm for GRB engines and there have been various implementations of this concept [13–17]. Recently Lyutikov and Blackman suggested that gamma-rays are emitted at the point where MHD breaks down due to the overturn instability of large amplitude electromagnetic wave [18].

In the present Letter we explore the mechanism for the localization of multi-dimensional intense EM radiation in pure e–p plasmas. Assuming the plasma to be transparent to the beam, and applying a fully relativistic hydrodynamical model, we demonstrate the possibility of beam self-trapping leading to the formation of stable 2D solitonic structures. The high-frequency pressure force of the EM field (tending to completely expel the pairs radially from the region of localization) is overwhelmed by the thermal pressure force which opposes the radial expansion of the plasma creating conditions for the formation of the stationary self-guiding regime of beam propagation.

2. Basic equations

In this section we apply our general formulation to the problem of self-trapping of EM beams in pure e–p plasmas with relativistic temperatures. We assume that the equilibrium state of the plasma is characterized by an overall charge neutrality $n_{\infty}^- = n_{\infty}^+ \equiv n_{\infty}$, where n_{∞}^- and n_{∞}^+ are the unperturbed number densities of the electrons and positrons in the far region of the EM beam localization. In most mechanisms for creating e–p plasmas, the pairs appear simultaneously and due to the symmetry of the problem it is natural to assume that $T_{\infty}^- = T_{\infty}^+ \equiv T_{\infty}$, where T_{∞}^- and T_{∞}^+ are the respective equilibrium temperatures.

We shall assume that for the radiation field of interest, the plasma is underdense and transparent, i.e., $\epsilon = \omega_e/\omega \ll 1$, where ω is the mean frequency of EM radiation and $\omega_e = (4\pi e^2 n_{\infty}/m_0 e)^{1/2}$ is the plasma frequency. Following Ref. [19] we introduce a temperature dependent momentum $\mathbf{\Pi}^{\pm} = G^{\pm} \mathbf{p}^{\pm}$ and relativistic factor $\Gamma^{\pm} = G^{\pm} \gamma^{\pm}$, where $G = K_3(z)/K_2(z)$ is the temperature dependent factor with K_n the n th order modified Bessel function of the second kind ($z = m_0 e c^2/T$), \mathbf{p}^{\pm} and $\gamma^{\pm} = \sqrt{1 + (\mathbf{p}^{\pm}/m_e c)^2}$ are respectively momentum and relativistic factor of e–p particles. Introducing the dimensionless quantities $\tilde{t} = \omega t$, $\tilde{\mathbf{r}} = (\omega/c)\mathbf{r}$, $\tilde{T}^{\pm} = T^{\pm}/m_0 e c^2$, $\tilde{\mathbf{A}} = e\mathbf{A}/(m_0 e c^2)$, $\tilde{\phi} = e\phi/m_0 e c^2$, $\tilde{\mathbf{\Pi}}^{\pm} = \mathbf{\Pi}^{\pm}/(m_0 e c)$, and $\tilde{n}^{\pm} = n^{\pm}/n_{\infty}$, we arrive at the dimensionless equations [19],

$$\frac{\partial \mathbf{\Pi}^{\pm}}{\partial t} + \nabla \Gamma^{\pm} = \mp \frac{\partial \mathbf{A}}{\partial t} \mp \nabla \phi, \quad (1)$$

$$\frac{n^{\pm}}{\Gamma^{\pm} f(T^{\pm})} = \text{const}, \quad (2)$$

$$\frac{\partial n^{\pm}}{\partial t} + \nabla \cdot \mathbf{J}^{\pm} = 0, \quad (3)$$

$$\Delta \phi = \epsilon^2 (n^- - n^+), \quad (4)$$

$$\frac{\partial^2 \mathbf{A}}{\partial t^2} - \Delta \mathbf{A} + \frac{\partial}{\partial t} \nabla \phi - \epsilon^2 (\mathbf{J}^+ - \mathbf{J}^-) = 0, \quad (5)$$

where

$$f(T^{\pm}) = \frac{K_2(1/T^{\pm})T^{\pm}}{G^{\pm}(T^{\pm})} \exp[G^{\pm}(T^{\pm})/T^{\pm}], \quad (6)$$

with $\mathbf{J}^{\pm} = n^{\pm} \mathbf{\Pi}^{\pm}/\Gamma^{\pm}$ and $\Gamma^{\pm} = \sqrt{(G^{\pm})^2 + (\mathbf{\Pi}^{\pm})^2}$. Here \mathbf{A} and ϕ are the vector and scalar potentials ($\nabla \cdot \mathbf{A} = 0$). The tilde is suppressed for convenience.

Of various techniques that could be invoked to investigate Eqs. (1)–(6) to study the self-trapping of high-frequency EM radiation propagating along the z -axis, we choose the method presented in the excellent paper by Sun et al. [20]. The method is based on the multiple scale expansion of the equations in the small parameter ϵ . Assuming that all variations are slow compared to the variation in $\xi = z - at$, we expand all quantities $Q = (\mathbf{A}, \phi, \mathbf{\Pi}^{\pm}, n^{\pm}, \dots)$ as

$$Q = Q_0(\xi, x_1, y_1, z_2) + \epsilon Q_1(\xi, x_1, y_1, z_2), \quad (7)$$

where $(x_1, y_1, z_2) = (\epsilon x, \epsilon y, \epsilon^2 z)$ denote the directions of slow change, and $a_1 = (a^2 - 1)/\epsilon^2 \sim 1$. We further assume that the high-frequency EM field is circularly polarized,

$$\mathbf{A}_{0\perp} = \frac{1}{2}(\hat{\mathbf{x}} + i\hat{\mathbf{y}})A \exp(i\xi/a) + \text{c.c.}, \quad (8)$$

where A is the slowly varying envelope of the EM beam, $\hat{\mathbf{x}}$ and $\hat{\mathbf{y}}$ denote unit vectors, and c.c. is the complex conjugate.

We now give a short summary of the steps in the standard multiple-scale methodology (Ref. [20]). In the lowest order in ϵ , the transverse (to the direction of EM wave propagation z) component of Eq. (1) reduces to

$$\mathbf{\Pi}_{0\perp}^{\pm} = \mp \mathbf{A}_{0\perp}. \quad (9)$$

To the next order (in ϵ), the transverse component of Eq. (1) reads:

$$-a \frac{\partial \mathbf{\Pi}_1^{\pm}}{\partial \xi} + \nabla_{\perp} \Gamma_0^{\pm} = \pm a \frac{\partial \mathbf{A}_1}{\partial \xi} \mp \nabla_{\perp} \phi_0. \quad (10)$$

Averaging Eq. (10) over the fast variable ξ we obtain $\nabla_{\perp} \Gamma_0^{\pm} = \mp \nabla_{\perp} \phi_0$. Using these relations, we obtain $\nabla_{\perp} \phi_0 = 0$ and

$$\Gamma_0 \equiv \Gamma_0^{\pm} = \text{const}. \quad (11)$$

Note that from the lowest order of Eqs. (2) and (4), we conclude that $n_0^+ = n_0^- \equiv n_0$ and $T_0^+ = T_0^- \equiv T_0$. The relation between EM field and temperature can be found by invoking Eq. (11). Using Eqs. (8) and (9) and determining integration constant such that $A \rightarrow 0$ and $T_0 \rightarrow T_{\infty}$, we obtain

$$G^2(T_0) = G^2(T_{\infty}) - |A|^2. \quad (12)$$

The equation for slowly varying envelope A of EM beam can be obtained from Eq. (5). To the lowest order we find

$$a_1 \frac{\partial^2 \mathbf{A}_{0\perp}}{\partial \xi^2} - \nabla_{\perp}^2 \mathbf{A}_{0\perp} - 2 \frac{\partial^2 \mathbf{A}_{0\perp}}{\partial \xi \partial z_2} + 2 \frac{n_0(T_0)}{G(T_{\infty})} \mathbf{A}_{0\perp} = 0. \quad (13)$$

In deriving this equation, we have used the relation

$$\Gamma_0 = \sqrt{G^2(T_0) + |A|^2} = G(T_{\infty}). \quad (14)$$

While from Eq. (2), we have

$$n_0(T_0) = \frac{f(T_0)}{f(T_{\infty})}. \quad (15)$$

Substituting Eq. (8) into Eq. (13) we find

$$2i \frac{\partial A}{\partial z} + \nabla_{\perp}^2 A + \frac{2}{G(T_{\infty})} [1 - n(T_0)] A = 0, \quad (16)$$

where subscripts for variables (x_1, y_1, z_2) are dropped for simplicity. We also assumed without loss of generality that $(a^2 - 1)/\epsilon^2 a^2 = 2/G(T_{\infty})$, which in dimensional units (provided that $a = \omega/kc$) coincides with the linear dispersion relation of the EM wave in an e–p plasma:

$$\omega^2 = k^2 c^2 + \frac{2\omega_e^2}{G(T_{\infty})}. \quad (17)$$

Thus, the dynamics of EM beams in hot relativistic e–p plasma has become accessible within the context of a generalized nonlinear Schrödinger equation (16).

We first seek the localized 2D soliton solutions of Eq. (16), and analyze the stability of such solutions. Making the self-evident renormalization of variables $z \rightarrow zG(T_{\infty})$, $r_{\perp} \rightarrow r_{\perp}\sqrt{G(T_{\infty})/2}$, Eq. (16) can be written as

$$i \frac{\partial A}{\partial z} + \nabla_{\perp}^2 A + \Psi A = 0, \quad (18)$$

where $\Psi = 1 - n_0(T_0)$ represents the generalized nonlinearity. The companion equation (15) can be viewed as a transcendental algebraic relation between T_0 and $|A|^2$, i.e. Ψ is an implicit function of $|A|^2$ [$\Psi = \Psi(|A|^2)$]. We note that Eq. (18) can be written in the Hamiltonian form $i\partial_z A = \delta H/\delta A^*$, where the Hamiltonian is

$$H = \int d\mathbf{r}_{\perp} [|\nabla_{\perp} A|^2 - F(|A|^2)], \quad (19)$$

and $F(t) = \int_0^t \Psi(t') dt'$. This implies that Eq. (18) conserves the Hamiltonian H in addition to the power (photon number) $N = \int d\mathbf{r}_{\perp} |A|^2$.

To find a stationary, nondiffracting axisymmetric solution, we use the representation of vector potential $A/A_c = U(r) \exp(i\lambda z)$, where $A_c = [G(T_{\infty})^2 - 1]^{1/2}$, $r = (x^2 + y^2)^{1/2}$ and λ is the nonlinear wave-vector shift. The radially dependent envelope $U(r)$ obeys a nonlinear ordinary differential equation:

$$\frac{d^2 U}{dr^2} + \frac{1}{r} \frac{dU}{dr} - \lambda U + \Psi(U^2)U = 0. \quad (20)$$

The profiles of the field $U(r)$, the plasma density $n_0(r)$, and the temperature $T_0(r)$ of the stationary solution can be found in Fig. 3 of Ref. [19] for $\lambda = 0.1$; The plasma temperature and density is reduced in the region of field localization. Similar plots could be obtained for all allowed values of λ . When $\lambda \rightarrow \lambda_c$, where λ_c is the upper bound of the propagation constant, the plasma cavitation takes place, i.e. the plasma density and temperature tends down to zero at $r = 0$. Appearance of zero temperature is not surprising since the corresponding region is the “plasma vacuum”; all particles are gone away.

The stability of obtained soliton solutions can be investigated using the stability criterion of Vakhitov and Kolokolov [21]. According to this criterion the soliton is stable against small arbitrary perturbations if

$$\frac{dN}{d\lambda} > 0, \quad (21)$$

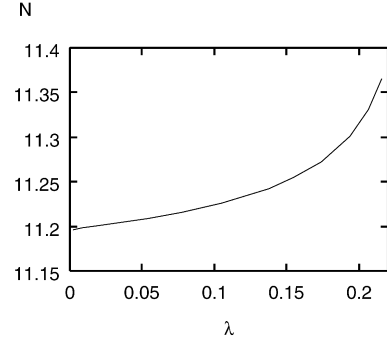


Fig. 1. The beam power N versus λ ($T_{\infty} = 1$).

where N is the photon number or more precisely the power of the trapped mode. In our case, the dependence of N on λ is shown in Fig. 1. One can see that $dN/d\lambda > 0$ everywhere and consequently the corresponding solution is stable for $0 < \lambda < \lambda_c$.

3. Nonlinear dynamics based on variational approach

The complex dynamics of a beam governed by Eq. (18) can be analyzed by the variational approach [22]. This approach determines the relations between the characteristic parameters of the localized solution approximated by a trial function. The variational method gives qualitatively good results, provided the beam does not undergo structural changes during its evolution. The first standard step is to construct the Lagrangian

$$L = \frac{1}{2} \left(A^* \frac{\partial A}{\partial z} - \text{c.c.} \right) - \mathcal{H}, \quad (22)$$

where \mathcal{H} is the Hamiltonian density [$H = \int d\mathbf{r}_{\perp} \mathcal{H}$, see Eq. (19)]. In the optimization procedure, the first variation of the variational function must vanish on a suitably chosen trial function. As a trial function, we will use the Gaussian-shaped beam,

$$A = \Lambda(z) \exp \left[-\frac{r^2}{2a(z)^2} + ir^2 b(z) + i\phi(z) \right], \quad (23)$$

with the amplitude Λ , the beam radius a , the wave front curvature b and the phase ϕ as the unknown functions of the propagation coordinate z respectively, which will be furthermore used in order to make the variational functional an extremum. Substituting expression (23) into Eq. (22) and demanding that the variation of the spatially averaged Lagrangian with respect to each of these parameters is zero, we obtain the corresponding set of Euler–Lagrange equations,

$$\frac{d}{dz} (\Lambda^2 a^2) = 0, \quad (24)$$

$$\frac{d^2 a}{dz^2} = \frac{4}{a^3} - \frac{2}{a} \left[K'(\Lambda^2) - \frac{K(\Lambda^2)}{\Lambda^2} \right], \quad (25)$$

$$b = \frac{1}{4a} \frac{da}{dz}, \quad (26)$$

to be solved for the three functions Λ , a , and b , where the function $K(u)$ is defined as

$$K(u) = 4 \int_0^\infty dp p F(ue^{-p^2}). \tag{27}$$

Eq. (24) is nothing but a statement of the fact that during the EM beam evolution its power is conserved,

$$N = \pi \Lambda^2 a^2 = \pi \Lambda_0^2 a_0^2, \tag{28}$$

where Λ_0 and a_0 are respectively the initial amplitude and the initial “radius” of the EM beam at $z = 0$.

Using Eq. (24), the integration of Eq. (25) leads to

$$\frac{1}{2} \left(\frac{da}{dz} \right)^2 + V(a) = H = V(a_0), \tag{29}$$

where

$$V(a) = \frac{2}{a^2} - \frac{2a^2}{a_0^2 \Lambda_0^2} K \left(\frac{\Lambda_0^2 a_0^2}{a^2} \right) \tag{30}$$

plays the role of an effective potential for the evolution of the radius a . We have assumed that the initial beam have a plane front (or zero curvature) [$da/dz|_{z=0} = 0 = b(0)$]. Using the analogy with a particle in a potential well, we can acquire a deeper physical understanding of light beam dynamics. Choosing the initial beam radius a_0 to be equal to the equilibrium radius a_e , a stationary solution of Eq. (29) is obtained if $\partial V/\partial a|_{a=a_e} = 0$. Note that $-\partial V/\partial a$ is equal to the right-hand side of Eq. (25). The equilibrium radius of the beam is readily found to be

$$a_e^2 = 2 \left[K'(\Lambda_0^2) - \frac{K(\Lambda_0^2)}{\Lambda_0^2} \right]^{-1}. \tag{31}$$

In the subsequent analysis we will consider the small temperature case $T_\infty \ll 1$, and the case of moderately high temperature $T_\infty \sim 1$. We do not consider here the ultrarelativistic temperature case ($T_\infty \gg 1$) because applied model equations fail to adequately describe the plasma dynamics due to the neglect of heavy particle production.

In the small temperature case the nonlinear term in Eq. (18) reduces to a simple analytic expression

$$\Psi(|A|^2) = 1 - (1 - |A|^2)^{3/2}, \tag{32}$$

which gives the function $F(u)$ as

$$F(u) = u + \frac{2}{5}(1 - u)^{5/2} - \frac{2}{5}. \tag{33}$$

We will apply the established general formalism to the saturating nonlinearity given by Eq. (32). The function K becomes [see Eq. (27)]

$$K(u) = 2u + \frac{4}{5} \left[(1 - u)^{1/2} \left(\frac{46}{15} - \frac{22u}{15} + \frac{2u^2}{5} \right) - \frac{8}{5} \arctan(1 - u)^{1/2} - \frac{4}{5} \log u - \frac{4}{5} \left(\frac{46}{15} - \log 4 \right) \right]. \tag{34}$$

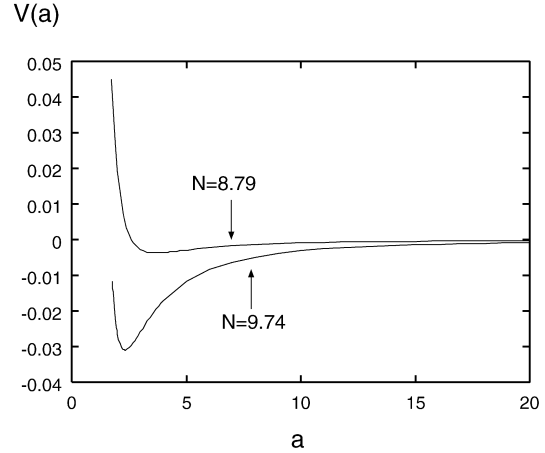


Fig. 2. Potential profile of $V(a)$ versus a in the case of $N = 8.79$ and $N = 9.74$.

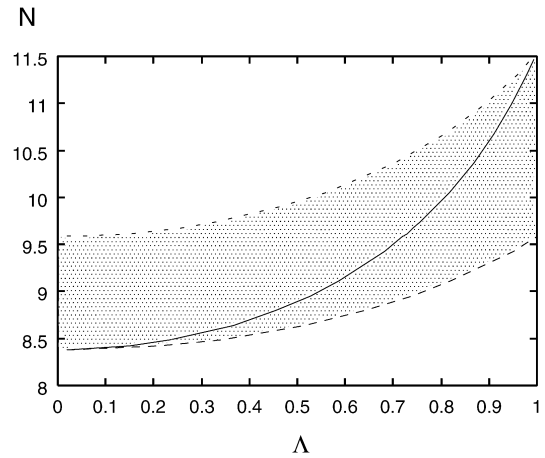


Fig. 3. The parameter regime where solitary wave can be trapped for $T_\infty \ll 1$.

Note that normalized strength of the field $A (= A/A_c)$ is restricted from above $|A| \leq 1$. Above this value the wave-breaking of the field takes place. Substituting Eq. (34) into Eq. (25), we can investigate the nonlinear dynamics of the beam for different initial conditions.

Using Eq. (34) we can find the effective potential $V(a)$ [see Eq. (30)]. The shape of effective potentials in the case of $N = 8.79$ and $N = 9.74$ are illustrated in Fig. 2. From the shape of the potential we conclude that the “effective particle” (i.e. the beam) can be trapped in the potential well. The endpoints of these lines (for small a) correspond to the occurrence of zero density. As a decreases the beam amplitude Λ increases and approaches the unity at endpoints. Note that the potential at the endpoint is negative for $N = 9.74$. Thus, the cavitation can take place when the initial radius a_0 is large enough. It is obvious that $a(z)$ is an oscillating function provided that a_0 is in the trapping region.

The beam never diffracts if $H < 0$ which coincides with the general criterion established by Zakharov et al. [23]. Fig. 3 shows the parameter regime where the solitary wave could be trapped. The central line denotes the equilibrium curve, and the shaded region between two dashed curves denotes a region where EM beam is trapped. The lower dashed line corresponds

to the zero Hamiltonian. Thus, below this line, the electromagnetic beam with any parameters will diffract. Above the upper dashed line, the electromagnetic beam amplitude will grow up to wave-breaking limit. Therefore, the beam will be trapped in oscillatory regime provided that its parameters are situated in shaded region in Fig. 3.

4. Numerical simulation

In the preceding analysis, we applied a variational approach involving a Gaussian trial function. The main limitation of this approach is that it is valid only in the aberration-less approximation, i.e. the approach is unable to account for structural changes in the beam shape. Such aspects of the beam dynamics are better delineated by numerical simulations. The detailed dynamics of arbitrary field distribution must be studied by direct simulations of Eq. (18). The guidelines for simulation are still provided by approximative analytical approaches.

The initial profile of the beam is taken to be Gaussian $A = A_0 \exp(-r^2/2a_0^2)$. In the case of small temperature $T_\infty = 0.01$ the initial parameters are taken in the trapping region shown in Fig. 3. The initial focusing or defocussing before reaching the equilibrium, can be seen in Fig. 4, where the z -propagations of the beam fields $|A(r=0, z)|$ with same initial power $N = 9.5$ but with different amplitudes $A_0 = 0.37$ and $A_0 = 0.95$ are simultaneously drawn. Corresponding initial states of the beams are respectively situated on the left and right side of equilibrium curve in Fig. 3. Fig. 4 shows that the beams parameters are oscillating around the equilibrium with initial focusing ($A_0 = 0.37$) or defocussing ($A_0 = 0.95$) in agreement with the prediction of variational approach.

Fig. 5 shows the field distribution versus radius r and the propagating coordinate z for $A_0 = 0.37$. Note, however, that due to the appearance of the radiation spectrum the amplitudes of the field oscillations are monotonically decreasing with increasing z . For larger z the formation of a ground solitonic state may take place due to the damp-out of the oscillations. If the initial profile of the beam is close to the equilibrium one, then the beam quickly reaches the profile of ground-state equilibrium,

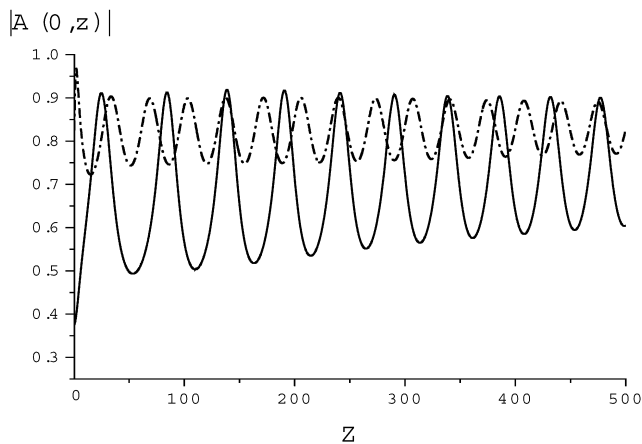


Fig. 4. The beams parameters are oscillating around the equilibrium with initial focusing ($A_0 = 0.37$) or defocussing ($A_0 = 0.95$).

and propagates for a long distance without much distortion of its shape. Since variational approach is unable to account the structural changes in the beam shape and corresponding formation of radiation spectra we can expect that the trapping region in (N, A_0) plane obtained by numerical simulations will be different from the one shown in Fig. 3. The result of these simulations is presented in Fig. 6. The curve ‘e’ corresponds to the equilibrium state, the curve ‘h’ the zero Hamiltonian, and the curve ‘t’ the trapping boundary, respectively. The Gaussian beam with initial parameters (i.e. N and A_0) in the region below line h has a positive Hamiltonian and will be diffracted. The trapping region of the beam is the area between lines h and t. The beam with the parameters in this region will be trapped in self-guiding regime of propagation and will either focus or defocus to the ground state, exhibiting damped oscillations around it. The initial focusing (defocussing) takes place if the parameters are in the region between lines t and e (between e and h). Note that the area of the trapping region shown in Fig. 6 is larger than it follows from variational approach (see Fig. 3). This enlargement of the trapping area is related to the radiation losses during the beam convergence to the equilibrium state.

The beam with parameters in region above trapping line t will focus until wave-breaking and plasma cavitation takes

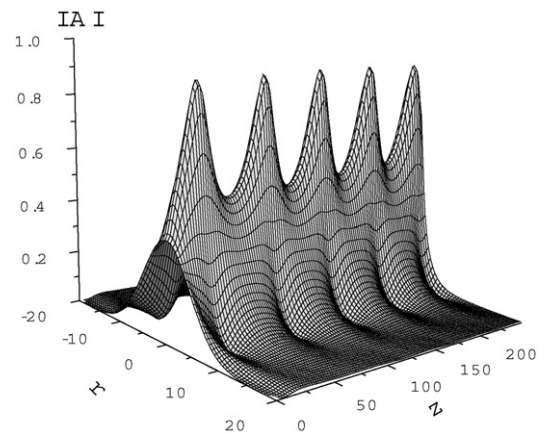


Fig. 5. The field distribution versus r and z for $A_0 = 0.37$.

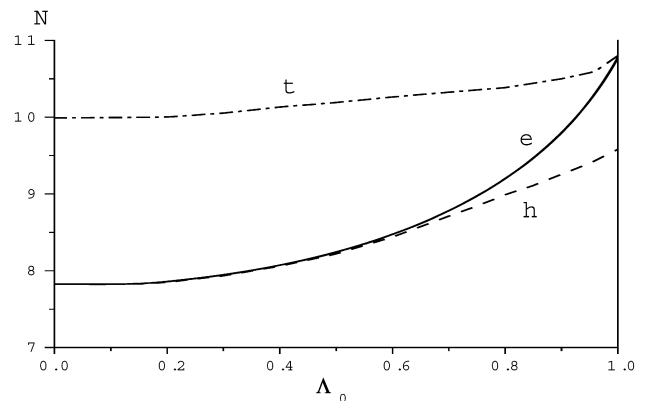


Fig. 6. The trapping region in (N, A_0) plane obtained by numerical simulations for $T_\infty \ll 1$. The curve ‘e’ corresponds to the equilibrium state, the curve ‘h’ the zero Hamiltonian, and the curve ‘t’ the trapping boundary, respectively.

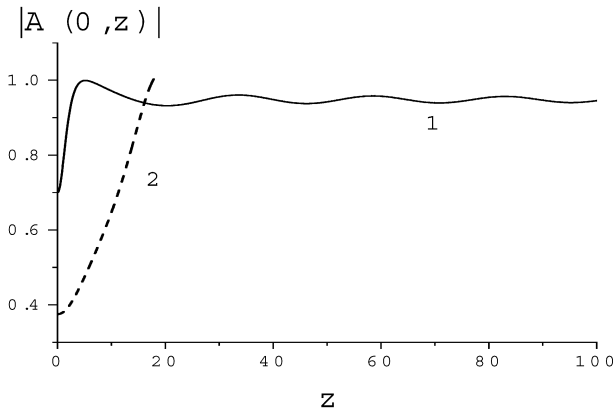


Fig. 7. The field $|A(r=0)|$ versus z for the cases when the beams parameters are in below (the curve 1) and above (the curve 2) the line t .

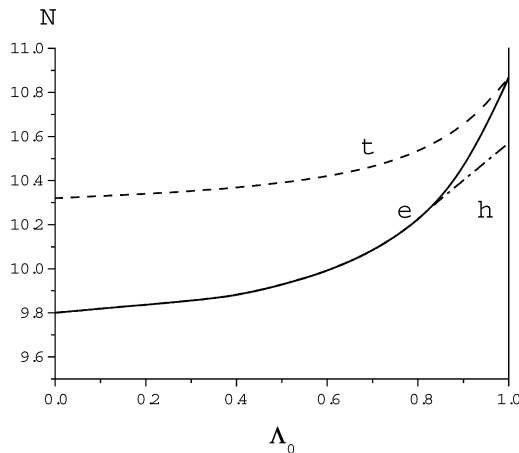


Fig. 8. The trapping region in (N, A_0) plane for $T_\infty = 0.3$ (the notations are same as in Fig. 6).

place. Fig. 7 shows the plot $|A(r=0)|$ versus z for the cases when the beams parameters are in the regions below (the curve 1) and above (the curve 2) the line t . One can see that in the first case the beam trapping takes place while, in the second case the beam amplitude increases up to the wave-breaking limit ($A = 1$).

For relativistic high temperature case the EM beam dynamics is similar to what we observed in the low temperature case. Fig. 8 shows the trapping region for $T_\infty = 0.3$ (the notations are same as in Fig. 6). Quantitative difference stems from the fact that in the high temperature case the mass of the e–p pairs are modified by the temperature dependent G -factor. It is interesting to mention that in this case in the region of field localization the plasma temperature can be decreased considerably. In Fig. 9 we demonstrate $T(r)$ versus z during the trapped beam evolution toward the stable equilibrium.

It is thus confirmed by numerical simulations that the beam trapping is robust especially for low background temperature regime. The beam can achieve the equilibrium state from a wide range of parameters, even far from the equilibrium, as it is predicted by our analytic approach. However, the area of trapping region reduces as temperature increases.

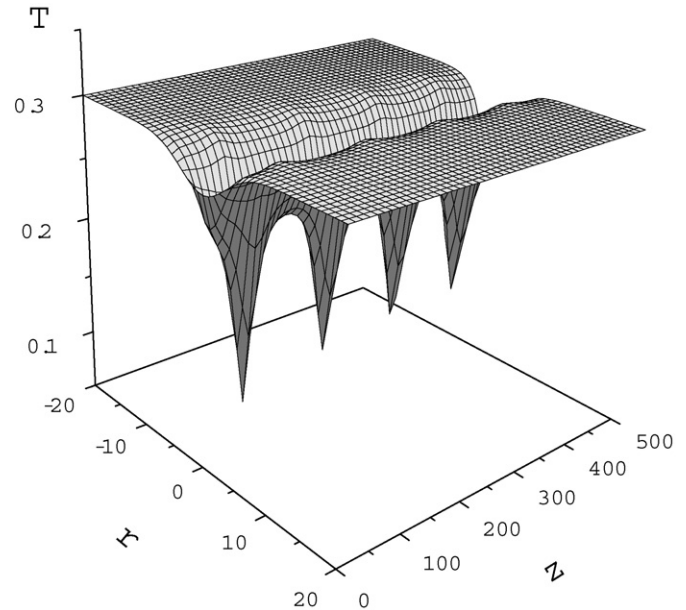


Fig. 9. The plasma temperature $T(r)$ versus z during the trapped beam evolution toward the stable equilibrium.

5. Summary

We have investigated the nonlinear propagation of strong 2D EM radiation in a relativistic, unmagnetized electron–positron plasma. The treatment is fully relativistic—in the thermal motion as well as in the coherent motion of the plasma particles. The fact that relativistically hot e–p plasmas are capable of sustaining high amplitude localized structures of high amplitude electromagnetic fields should be important to understand the complex radiative properties of different astrophysical objects where such plasmas are considered to exist.

By applying a variational technique with a Gaussian trial function, we have demonstrated the possibility of different regimes of EM beam propagation. In particular, the trapped beam exhibits an oscillatory behavior around the stationary solution. However, since the system contains an upper bound of the field amplitude, the parameter regime is restricted for these oscillations. If the initial beam intensity is large enough, the ponderomotive force acts strongly leading to the beam over-focusing, and eventually the EM field gives rise to the plasma cavitation and wave-breaking.

The region in parameter space where the beam can be regularly trapped and oscillate is found. We have also performed the numerical simulations and demonstrated the parameter regime where beam trapping takes place. Comparing the results of variational approach and the results of numerical simulations we have confirmed that analytical estimate gives a qualitatively good prediction for nonlinear wave dynamics. Due to the radiation and self-deformation of the beam, however, it is shown that the beam may be more robust than it follows from variational method.

In our consideration effects related to the temporal reshaping of the radiation have been ignored. However, we can easily generalize our results by allowing a temporal variation of the field.

If we assume that A weakly depends on $\tau = t - z/a$, Eq. (18) acquires an additional term related to the wave group velocity dispersion [$\sim (\omega_e^2/\omega^2)\partial^2 A/\partial\tau^2$]. In transparent plasma case this term can affect the long time dynamics of self-guiding channel. In particular due to weak modulation instability [24] the self-trapped beam eventually will break into a train of spatiotemporal solitons, i.e. the light bullets. Since general dynamical properties of the light bullet formation should not be sensitive to the type of saturating nonlinearity [25,26], we expect similar behavior of the EM beams in our case as well.

We may apply the present results to verify variety of GRB models. The obtained results could be useful to understand the radiative properties of astrophysical objects like the AGN, the pulsars and extragalactic electron–positron Jets.

Acknowledgements

The work of V.I.B. and S.V.M. was partially supported by ISTC and Georgian NSF.

References

- [1] P.A. Sturrock, *Astrophys. J.* 164 (1971) 529;
M.A. Ruderman, P.G. Sutherland, *Astrophys. J.* 196 (1995) 51;
F.C. Michel, *Theory of Neutron Star Magnetospheres*, University of Chicago Press, Chicago, 1991.
- [2] M.C. Begelman, R.D. Blandford, M.J. Rees, *Rev. Mod. Phys.* 56 (1984) 255.
- [3] M.L. Burns, in: M.L. Burns, A.K. Harding, R. Ramaty (Eds.), *Positron–Electron Pairs in Astrophysics*, American Institute of Physics, New York, 1983.
- [4] S. Weinberg, *Gravitation and Cosmology*, Wiley, New York, 1972;
- P.J.E. Peebles, *Principles of Physical Cosmology*, Princeton Univ. Press, Princeton, 1993.
- [5] M. Perry, G. Mourou, *Science* 264 (1994) 917;
S.P. Hatchett, et al., *Phys. Plasmas* 7 (2000) 2076.
- [6] A.C.L. Chian, C.F. Kennel, *Astrophys. Space Sci.* 97 (1983) 9.
- [7] R.E. Kates, D.J. Kaup, *J. Plasma Phys.* 41 (1989) 507.
- [8] R.T. Gangadhara, V. Krishan, P.K. Shukla, *Mon. Not. R. Astron. Soc.* 262 (1993) 151.
- [9] T. Tajima, T. Taniuti, *Phys. Rev. A* 42 (1990) 3587;
K. Holcomb, T. Tajima, *Phys. Rev. D* 40 (1989) 3909.
- [10] V.I. Berezhiani, S.M. Mahajan, *Phys. Rev. Lett.* 73 (1994) 1110;
V.I. Berezhiani, S.M. Mahajan, *Phys. Rev. E* 52 (1995) 1968.
- [11] T. Tatsuno, V.I. Berezhiani, S.M. Mahajan, *Phys. Rev. E* 63 (2001) 046403;
T. Tatsuno, V.I. Berezhiani, M. Pekker, S.M. Mahajan, *Phys. Rev. E* 68 (2003) 016409.
- [12] M.J. Rees, astro-ph/9701162.
- [13] V.V. Usov, *Nature* 357 (1992) 472.
- [14] C. Thompson, *Mon. Not. R. Astron. Soc.* 270 (1994) 480.
- [15] E.G. Blackman, L. Yi, G.B. Field, *Astrophys. J.* 473 (1996) L79.
- [16] P. Mészáros, M.J. Rees, *Astrophys. J.* 482 (1997) L29.
- [17] W. Kluzniak, M.A. Ruderman, *Astrophys. J.* 505 (1998) 113.
- [18] M. Lyutikov, E.G. Blackman, *Mon. Not. R. Astron. Soc.* 321 (2001) 177.
- [19] V.I. Berezhiani, S.M. Mahajan, Z. Yoshida, M. Ohhashi, *Phys. Rev. E* 65 (2002) 047402.
- [20] G.Z. Sun, E. Ott, Y.C. Lee, P. Guzdar, *Phys. Fluids* 30 (1987) 526.
- [21] N.G. Vakhitov, A.A. Kolokolov, *Izv. Vyssh. Uchebn. Zaved. Radiofiz.* 16 (1973) 1020, *Sov. Radiophys.* 9 (1973) 262.
- [22] V. Skarka, V.I. Berezhiani, R. Miklaszewski, *Phys. Rev. E* 56 (1997) 1080.
- [23] V.E. Zakharov, V.V. Sobolev, V.C. Synakh, *Zh. Eksp. Teor. Fiz.* 60 (1971) 136, *Sov. Phys. JETP* 33 (1971) 77.
- [24] V.E. Zakharov, A.M. Rubenchik, *Zh. Eksp. Teor. Fiz.* 65 (1973) 997, *Sov. Phys. JETP* 38 (1974) 494.
- [25] S.M. Mahajan, V.I. Berezhiani, R. Miklaszewski, *Phys. Plasmas* 5 (1998) 3264.
- [26] P.K. Shukla, M. Marklund, B. Eliasson, *Phys. Lett. A* 324 (2004) 193.